

Article

Viscoelastic Characteristics and Mechanical Performances of Asphalt Mastic and Mixtures with Fly Ash from Municipal Solid Waste Incineration Residues

Ling Xu ¹, Yinfei Du ², Salvatore Bruno ³, Giuseppe Loprencipe ³ and Laura Moretti ^{3,*}

¹ Key Laboratory of Road and Traffic Engineering of Ministry of Education, Tongji University, No. 4800 Cao'an Road, Jiading District, Shanghai 201804, China

² School of Civil Engineering, Central South University, Changsha 410075, China

³ Department of Civil, Constructional and Environmental Engineering, Sapienza University of Rome, Via Eudossiana 18, 00184 Rome, Italy; salvatore.bruno@uniroma1.it (S.B.); giuseppe.loprencipe@uniroma1.it (G.L.)

* Correspondence: laura.moretti@uniroma1.it; Tel.: +39-064-458-5120

Abstract: The extraction and utilization of non-renewable mineral resources impose significant transportation and economic challenges in infrastructure construction. At the same time, recycling fly ash derived from the bottom ash in municipal solid waste incineration residues (MSWIRs) presents a waste management hurdle. This study investigates the viscoelastic characteristics and mechanical performances at different scales of asphalt mastic and mixture with fly ash from MSWIRs. Firstly, Fourier transform infrared spectrometry (FTIR) was adopted to distinguish the physically blended states of asphalt and fillers. Then, a frequency test using a dynamic shear rheometer (DSR) was conducted to construct viscoelastic master curves, focusing on asphalt mastic. A dynamic modulus test characterized the viscoelastic behavior at the asphalt mixture scale. Furthermore, the mechanical performances of asphalt mixtures were evaluated, including the resilient modulus through indirect tension tests, moisture susceptibility via the immersed Marshall stability test, and anti-cracking properties with a low-temperature bending test. The FA incorporation in the mixture decreased the immersion residual stability by 7.40%, and increased the flexural tensile strength by 5.03% and the stiffness modulus by 78.67%. The mechanical evaluation of the mixture with FA could meet the application requirements of the asphalt layer. Finally, statistical analyses were conducted to present strong correlations (coefficient R^2 over 0.70) among the mechanical results. Fly ash in asphalt mixtures revealed potential as a sustainable approach for waste reuse in road construction. Additionally, substituting mineral fillers at the mastic scale significantly influences the viscoelastic characteristics and mechanical performances of asphalt materials at the mixture scale.

Keywords: asphalt pavements; green technologies; waste recycling; fly ash; MSWIRs; viscoelastic characteristics; mechanical performances



Citation: Xu, L.; Du, Y.; Bruno, S.; Loprencipe, G.; Moretti, L. Viscoelastic Characteristics and Mechanical Performances of Asphalt Mastic and Mixtures with Fly Ash from Municipal Solid Waste Incineration Residues. *Buildings* **2024**, *14*, 672. <https://doi.org/10.3390/buildings14030672>

Academic Editor: Antonio Caggiano

Received: 30 January 2024

Revised: 27 February 2024

Accepted: 1 March 2024

Published: 3 March 2024



Copyright: © 2024 by the authors. Licensee MDPI, Basel, Switzerland. This article is an open access article distributed under the terms and conditions of the Creative Commons Attribution (CC BY) license (<https://creativecommons.org/licenses/by/4.0/>).

1. Introduction

Fly ash can be mainly classified as coal-burnt fly ash and fly ash derived from the bottom ash in municipal solid waste incineration residues (MSWIRs) [1,2]. Fly ash derived from MSWIRs' bottom ash is a by-product of waste burning in thermal power plants [1]. They are produced through the rapid expansion of some gases (e.g., nitrogen, hydrogen, and carbon dioxide) in the molten clay mineral droplets during the waste-burning process [2]. MSWIRs have an extremely low density ($<0.8 \text{ g/cm}^3$), hollow structure, and spherical particles, making them difficult for landfill disposal [3].

Fly ash has been widely used in civil engineering for pavements, buildings, and constructions. It is reported to enhance pozzolanic reactions in concrete [4–6]. Road construction is the main application area of fly ash [7,8]. The rational use of fly ash in

asphalt can also solve the problems of environmental pollution [9,10] and land resource occupation [11,12]. Therefore, a systematic evaluation of the properties of asphalt materials containing fly ash is necessary to facilitate practical applications.

Moreover, the traffic channelization on the expressway is increasing [13]. These changes in traffic conditions brought critical conditions to asphalt pavements, resulting in early rutting and damage [14,15]. Therefore, the pavement decay level accelerates, and the service life is shortened, causing economic losses and constituting safety hazards for traffic [16,17].

Due to the wide range of factors affecting the thermal and mechanical properties of asphalt, damage prevention in flexible pavement has emerged as a global challenge [18,19]. In the literature, several studies designed and developed high- and low-temperature performance tests [20–22] to simulate actual conditions [23]. The dynamic shear rheological (DSR) method considers the effects of temperature and loading time by measuring the strain, stress, load frequency, temperature, and time during the test [24]. The rheological properties of asphalt [24] are evaluated using phase angle, modulus, rutting factor, fatigue factor, loss factor (damping), viscosity, and compliance.

In the realm of asphalt mixture testing, standard procedures such as the rutting test are commonly employed to evaluate the high-temperature performance of asphalt mixtures. However, field applications have revealed that even when the results of rutting tests conform to specified standards, the guarantee of high-temperature stability in the pavement during service remains uncertain [25]. According to an NCHRP report, the flow number (Fn) describes the boundary points of the second and third stages in the permanent strain curve of the asphalt mixture [26,27]. The greater the Fn, the smaller the creep damage probability, and the results of the flow number test correlate with the rut depth [28,29].

Simple performance metrics cannot describe asphalt behavior [30], and the viscoelastic characteristics and phase transformation of asphalt have to be evaluated in the full temperature range [31] by varying its composition [32]. The incorporation of fly ash as mineral powder modifies the properties at the scale of the asphalt mastic and mixture [33,34]. The mechanical properties of concrete will also change accordingly [35,36]. In previous studies, fly ash has been applied to cement concrete, and its hydration reaction has been tested [37,38]. Yinfei et al. investigated the application of fly ash as a filler in asphalt mixtures and focused on the service performance [3]. The stiffness of cement concrete and the flexibility of asphalt concrete result in different mechanical properties, and the role of fly ash in them must be assessed according to the constitutive differences between the various materials [39].

Therefore, this study investigates the feasibility of reusing fly ash from MSWIRs in asphalt pavements by investigating its viscoelastic [40] characteristics and mechanical performances at different scales of mastic and mixture. Based on an equal volume concept, fly ash was incorporated into the mixture as a filler to replace the limestone filler, and five kinds of asphalt mixtures were prepared. Fourier transform infrared spectrometry was adopted to distinguish the physically blended states of asphalt and fillers. Then, a frequency test was conducted to establish the viscoelastic master curves from the perspective of asphalt mastic. The dynamic modulus test described the viscoelastic behavior at the scale of the asphalt mixture. The mechanical performances of asphalt mixtures were evaluated comprehensively, including the resilient modulus with an indirect tension test, the moisture susceptibility with an immersed Marshall stability test, and anti-cracking properties with a low-temperature bending test.

2. Materials and Methods

2.1. Materials

2.1.1. Aggregates and Fillers

In this study, the limestone filler (LF) and fly ash (FA) from MSWIRs were used as the mineral powder for asphalt. LF (density equal to 2.77 g/cm^3) and FA (density equal to 0.72 g/cm^3) were passed at 0.075 mm sieve, according to T 0352-2000 [41]. The surface and

particle characteristics of the two fillers were measured using scanning electron microscope (SEM) with a magnification of 800 times (Figure 1). In addition, limestone (0–2.36 mm particle size) and diabase aggregates (2.36–13.2 mm particle size) were added to the mixtures. The mixtures were composed of 42.6% diabase aggregates (9.5 to 13.2 mm), 29.4% diabase aggregates (2.36 and 9.5 mm), and 17.5% limestone aggregates (0 to 2.36 mm).

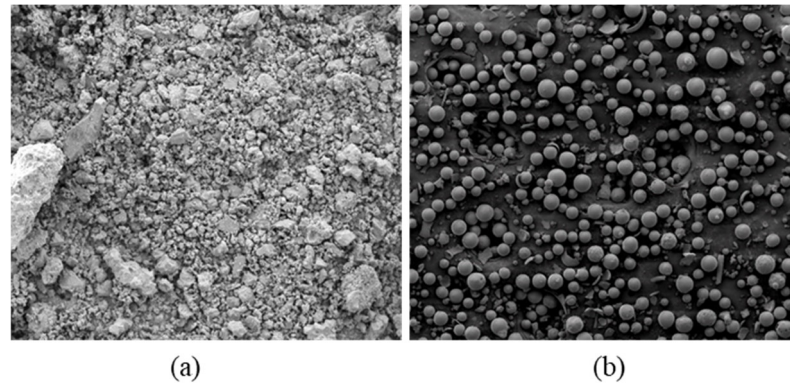


Figure 1. SEM picture with 800× magnification. (a) Limestone filler; (b) fly ash.

2.1.2. Bitumen

Table 1 lists the basic properties of PG 76-22 bitumen used in this study [42].

Table 1. Properties of PG 76-22 bitumen.

Property	Unit	Result	Technical Requirement	Standard
Penetration, 25 °C, 100 g/5 s	0.1 mm	68	60–80	T 0604 [42]
Softening point	°C	49.3	≥45	T 0606 [42]
Ductility, 5 °C	cm	>100	≥100	T 0605 [42]
Specific gravity	g/cm ³	1.087	-	T 0603 [42]

2.1.3. Asphalt Mastic and Mixture

The asphalt mixture SMA-13 [43] was used in this study. Table 2 lists the aggregate gradation of SMA-13 for the asphalt mixture. The control groups were set up to evaluate the impact of fly ash replacing mineral powder as a filler on the mixture performance according to [44].

Table 2. Aggregate gradation of asphalt mixture.

Sieve size/mm	16.0	13.2	9.5	4.75	2.36	1.18	0.6	0.3	0.15	0.075
Passing ratio/wt.%	100	90.3	63.0	26.8	17.4	15.3	13.4	11.2	10.8	9.8

Mastic #0 to Mastic #4 were prepared in this study. Based on an equal volume concept, FA filler replaced LF in the mastics and mixtures (Table 3).

Table 3. Filler volume ratio in asphalt mastic and mixture.

Mastic Type	Mixture Type	LF	FA
Mastic #0	Mixture #0	100%	0%
Mastic #1	Mixture #1	75%	25%
Mastic #2	Mixture #2	50%	50%
Mastic #3	Mixture #3	25%	75%

2.2. Test Methods

2.2.1. Fourier Transform Infrared (FTIR) Spectrometry

In this study, the attenuated total reflection Fourier transform infrared spectrometer (ATR-FTIR Bruker TENSOR 27, SpectraLab Scientific Inc., Markham, ON, Canada) allowed the investigation of molecular-level modification mechanisms in emulsified asphalt. This was achieved by analyzing variations in the absorption spectrum, which reflect changes in functional groups and their concentrations. The ATR-FTIR scans were conducted with a resolution of 4 cm^{-1} , covering a spectral range from 500 cm^{-1} to 3000 cm^{-1} . This technique was pivotal in quantitatively assessing the changes in specific functional groups, thereby elucidating the chemical properties of the emulsified asphalt.

2.2.2. Frequency Sweep Test

The mechanical behavior of viscoelastic materials can be expressed as a function of temperature and time domains. The frequency sweep test was performed at $40 \text{ }^\circ\text{C}$, $60 \text{ }^\circ\text{C}$, and $80 \text{ }^\circ\text{C}$ with $0.1\text{--}100 \text{ Hz}$ frequency range and 1% strain to investigate the linear viscoelastic behavior. Based on the principle of time–temperature equivalence, a reference temperature is selected, and the phase angle or dynamic modulus curves of asphalt at other different temperatures are translated into a smooth curve through calculation of the shift factor (α_T) from Equation (1) [3].

$$\log \alpha_T = \frac{C_1(T - T_0)}{C_2 + T - T_0} \quad (1)$$

where T is the test temperature; T_0 is the reference temperature; and C_1 and C_2 are fitting constants.

The reduction frequency (f_r) and the actual loading frequency (f) at T are calculated according to Equation (2) [3].

$$\lg f_r = \lg f + \lg \alpha_T = \lg f + \frac{E_a}{19.14714} \left(\frac{1}{T} - \frac{1}{T_0} \right) \quad (2)$$

where E_a is the activation energy.

After applying the shift factor α_T , the least squares method was used to fit the Sigmoidal equation [27] and obtain the master curve (Equation (3)).

$$\lg |E^*| = \theta + \frac{\alpha - \theta}{1 + e^{\beta + \gamma \cdot \lg f_r}} \quad (3)$$

where E^* is the measured dynamic modulus; θ is the minimum value of the dynamic modulus; α is the maximum value of the dynamic modulus; and β and γ are regression parameters representing the shape of the dynamic modulus master curve.

The master curves of asphalt mastics were also established by applying a double-logistic model [27] according to Equation (4).

$$\delta = \delta_p - \delta_p H(f_r - f_p) \left(1 - e^{-(S_R \log(\frac{f_r}{f_p}))^2} \right) + \delta_L H(f_p - f_r) \left(1 - e^{-(S_L \log(\frac{f_p}{f_r}))^2} \right) \quad (4)$$

where δ is the phase angle; H is the Heaviside step function; δ_p is the plateau of δ ; f_p is the frequency as δ_p occurred; S_R is the right master curve slope of δ beside plateau and S_L is the left master curve slope of δ beside plateau.

2.2.3. Dynamic Modulus Test

According to AASHTO TP 62-07 [45], the dynamic modulus test of asphalt mixture was conducted within frequency ranges from 0.1 Hz to 25 Hz at $-10 \text{ }^\circ\text{C}$, $4.4 \text{ }^\circ\text{C}$, $21.1 \text{ }^\circ\text{C}$, $37.8 \text{ }^\circ\text{C}$, and $54.4 \text{ }^\circ\text{C}$. The testing process in Figure 2 consisted of a stress control method with cylindrical specimens formed by a rotary compactor and cut into standard specimens

(i.e., 150 mm high and 100 mm diameter). Three sensors were attached to the side of the specimen at 120° intervals and 100 mm spacing.

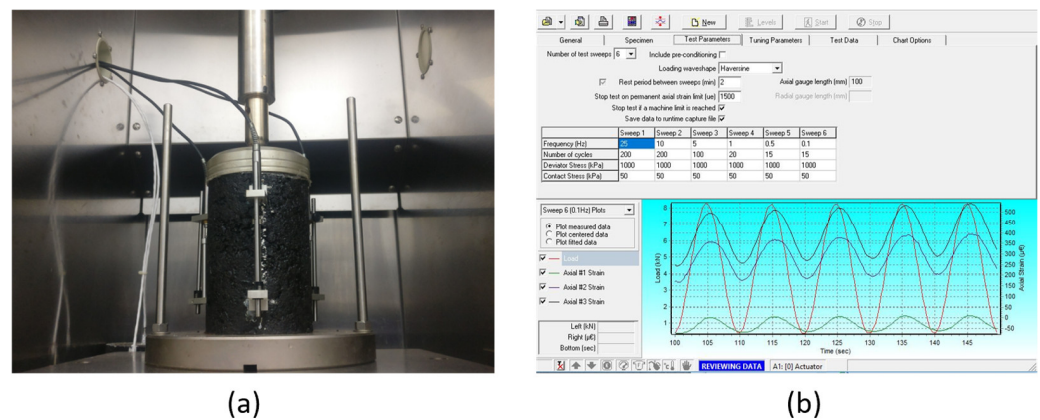


Figure 2. Dynamic Modulus test process. (a) Testing device; (b) testing data acquisition interface.

2.2.4. Resilient Modulus Test

The design method of asphalt pavements usually adopts the elastic layered system theory, based on the assumption of material isotropy [43]. However, the actual stress state of asphalt pavements exhibited a difference between the upper (compression stress zone) and bottom layer (tension stress zone) [46]. According to ASTM D7369-20 [47], the resilient modulus of the asphalt mixture was measured with the indirect tension module test. The test was performed at 5 °C, 25 °C, and 40 °C at 1 Hz frequency intervals with a Universal Testing Machine (UTM) (Figure 3). Two linear variable differential transducers (LVDTs) were used to monitor the horizontal deformation caused by vertical semi-sinusoidal loads on the diametric plane of samples. The resilient modulus M_r was calculated according to Equation (5).

$$M_r = \frac{F(v + 0.2734)}{H \times L} \quad (5)$$

where F is the maximum repeated vertical force, H is the recoverable deformation, L is the specimen thickness, and v is the Poisson ratio (i.e., 0.35 for asphalt).

2.2.5. Immersed Marshall Stability Test

Moisture damage is one of the major diseases of asphalt pavements [48]. It occurs when asphalt pavement is subjected to water or freeze–thaw cycles. Due to the dynamic load of vehicles, the moisture entering the pavement gaps generates dynamic water pressure or vacuum negative pressure suction [49]. At the interface of the aggregate, the adhesion of the asphalt is reduced, and the bonding force is gradually lost [29]. The process results in potholes, pushing, blistering, and deformation of the asphalt layer. The immersed Marshall stability test allowed calculating the immersion residual stability index (MS_0) of the specimens according to T 0709-2011 [42] (Equation (6)):

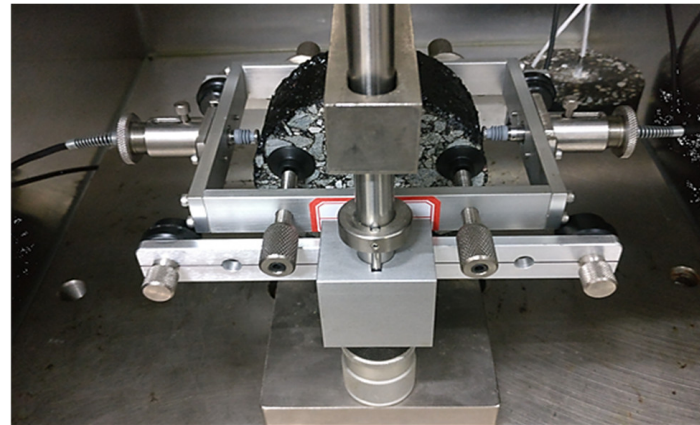
$$MS_0 = \frac{MS_1}{MS} \times 100 \quad (6)$$

where MS_1 is the stability after 48 h of water immersion at 60 °C, and MS is the initial stability.

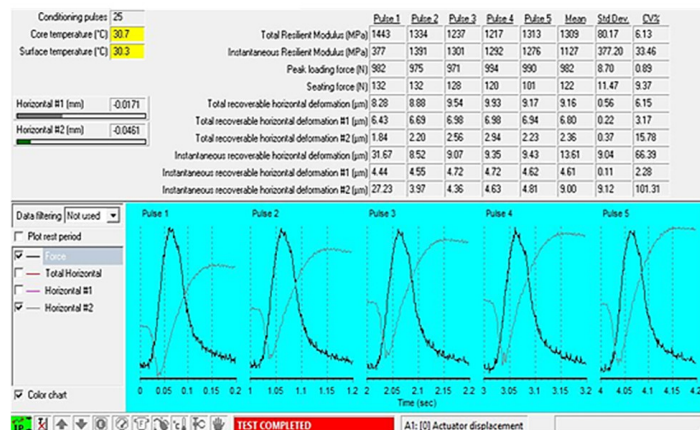
2.2.6. Bending Test

Pavement crack is a common disease that leads to a significant reduction in mixture strength and affects the performance of the pavement until its destruction [50]. The bending test is generally used to evaluate the low-temperature crack resistance of asphalt mixture. The bending test at −10 °C according to T 0715-2011 [42] allowed the calculation of the

tensile properties and cracking performance at low temperatures. Prismatic specimens were subjected to a three-point bending test at a 50 mm/min loading rate until failure (Figure 4).



(a)



(b)

Figure 3. Resilient modulus test. (a) Testing device; (b) data acquisition interface.



(a)



(b)

Figure 4. Bending test. (a) Before failure; (b) after failure.

The bending strength (R_B), maximum bending strain (ϵ_B), and the bending stiffness modulus (S_B) were calculated according to Equations (7) to (9), respectively.

$$R_B = \frac{3LP_B}{2bh^2} \tag{7}$$

$$\varepsilon_B = \frac{6hd}{L^2} \quad (8)$$

$$SB = \frac{R_B}{\varepsilon_B} \quad (9)$$

where L , h , and b are the support span, depth, and width of the specimen, respectively, P_B is the maximum load on the deflection curve, and d is the maximum deflection.

2.3. Statistical Analysis

In this study, statistical analysis was conducted with the Pearson correlation test. At a significance level of 5%, Equation (10) gave the correlation coefficient (R^2):

$$R^2 = \frac{\sum_{i=1}^n (X_i - \bar{X}) \times (Y_i - \bar{Y})}{\sqrt{\sum_{i=1}^n (X_i - \bar{X})^2} \times \sqrt{\sum_{i=1}^n (Y_i - \bar{Y})^2}} \quad (10)$$

where n is the number of samples, X_i and Y_i are the values of the two variables under investigation, respectively, and \bar{X} and \bar{Y} are the average values of the two variables, respectively.

3. Results and Discussions

3.1. FTIR Spectrum

Figure 5 shows the FTIR spectra of limestone and fly ash fillers with wavenumbers between 400 and 4000 cm^{-1} .

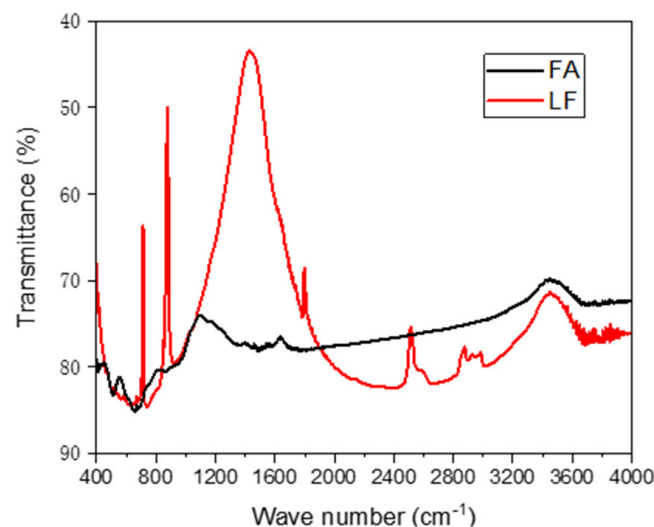


Figure 5. FTIR spectra of limestone and fly ash.

LF had strong sharp absorption peaks near 700 cm^{-1} and 850 cm^{-1} and a strong smooth absorption peak near 1450 cm^{-1} and 1800 cm^{-1} . Moreover, there was a weak sharp absorption peak near 2490 cm^{-1} , a weak small peak continuously distributed near 2830–2970 cm^{-1} , and a weak smooth absorption peak near 3400 cm^{-1} . On the other hand, fly ash had weak, rounded absorption peaks with smaller openings near 830 cm^{-1} and 1640 cm^{-1} . Additionally, there was a weak, rounded absorption peak with a large opening near 1120 cm^{-1} and 3410 cm^{-1} .

The FTIR spectra of asphalt without filler, mastic #0 with LF, and mastic #4 with FA are shown in Figure 6.

Asphalt mastic #0 and mastic #4 had very similar absorption peaks near wave numbers 1380 cm^{-1} , 1460 cm^{-1} , 2850 cm^{-1} , and 2920 cm^{-1} . Mastic #0 (Figure 6a) had new absorption peaks near wave numbers 700 cm^{-1} and 850 cm^{-1} , showing the specific absorption characteristics of LF. The FTIR spectrum of mastic #4 (Figure 6b) had no new absorption

peak in the range of measurement and confirmed the specific absorption characteristic of FA.

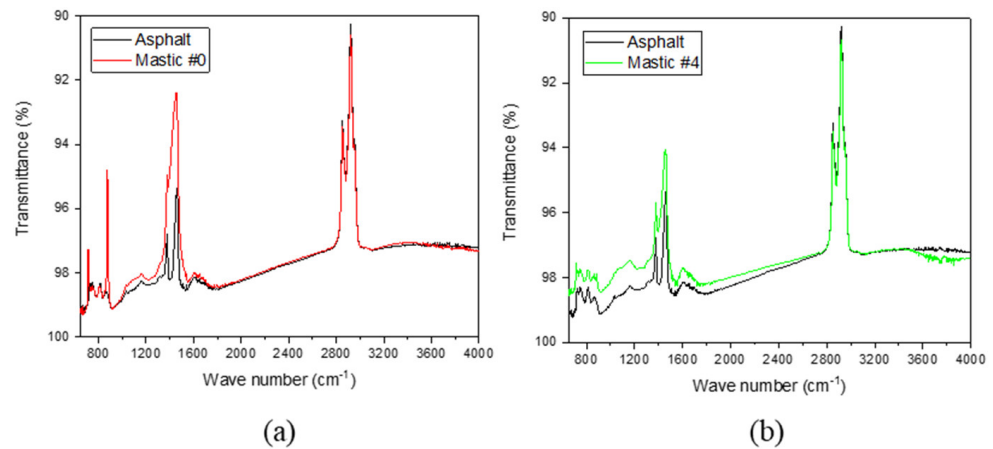


Figure 6. FTIR spectra. (a) Asphalt without filler and mastic #0; (b) asphalt and mastic #4.

Mastics with LF and FA had the characteristic absorption peaks of asphalt and mineral powders. During the mixing process, FA, LF, and bitumen were blended without chemical reactions, indicating that mineral powder and bitumen are compatible.

3.2. Master Curve of Asphalt Mastics

Figure 7a,b show the establishment process of the master curves of the complex shear modulus (G^*) and the phase angle (δ) of mastic #0.

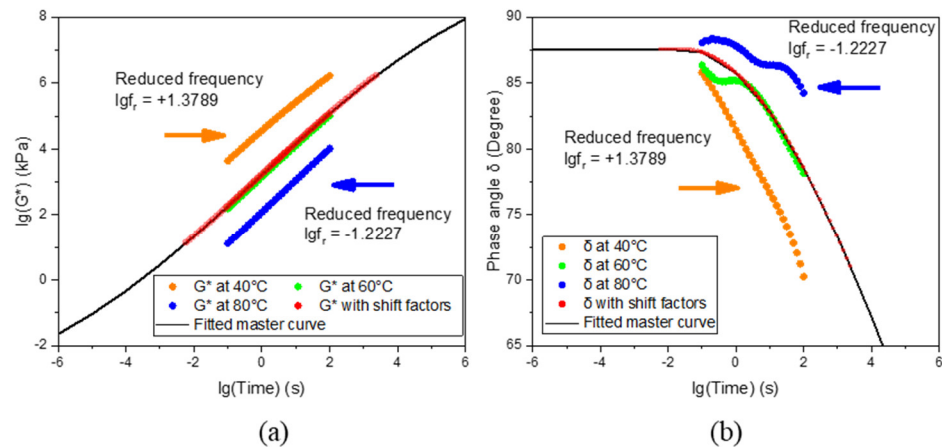


Figure 7. Master curves. (a) Complex shear modulus; (b) phase angle.

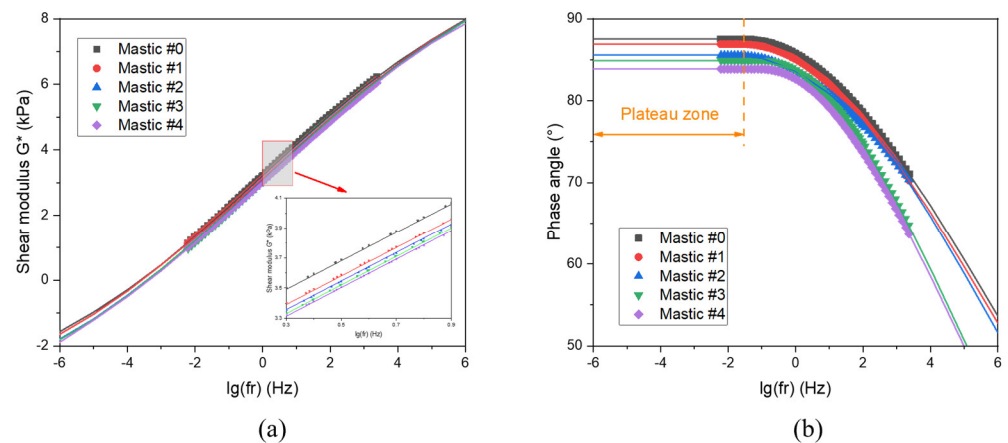
Correspondingly, Tables 4 and 5 list the fitting parameters of the master curves of G^* and δ for mastics, respectively. Figure 8 shows the fitting results of the master curves for various asphalt mastics.

Table 4. Fitting parameters of master curves of G^* —asphalt mastics.

Asphalt Mastic	FA Content [%]	α [kPa]	β [kPa]	γ [-]	θ [-]	E_a [J·mol ⁻¹]	R^2 [-]
Mastic #0	0%	11.690	-0.0409	-0.2644	-4.2830	137,720	0.9986
Mastic #1	25%	11.018	0.0577	-0.2602	-4.2881	137,134	0.9986
Mastic #2	50%	10.934	-0.0071	-0.2430	-4.3313	136,914	0.9987
Mastic #3	75%	10.409	-0.0071	-0.2403	-4.8496	136,215	0.9986
Mastic #4	100%	10.318	-0.0056	-0.2146	-5.6574	135,668	0.9987

Table 5. Fitting parameters of master curves of δ —asphalt mastics.

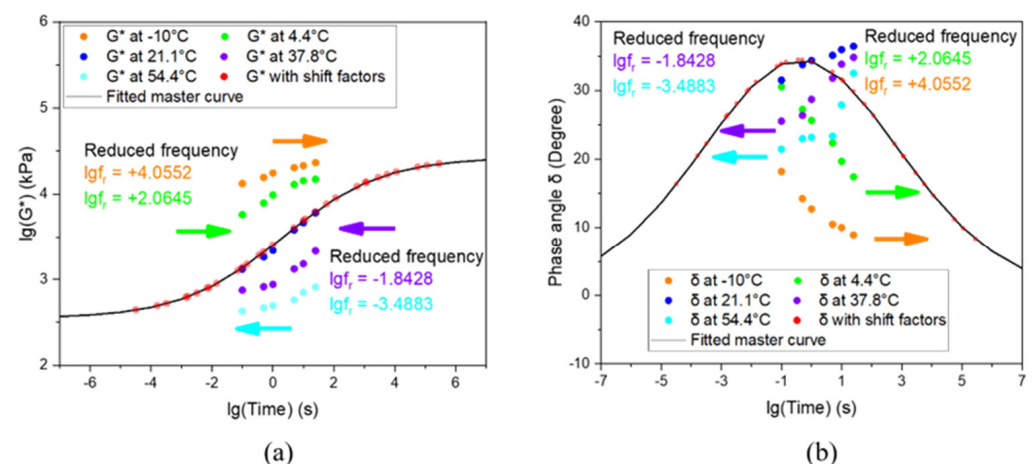
Asphalt Mastic	FA Content [%]	δ_p [°]	$\lg f_p$ [Hz]	S_L [-]	S_R [-]	R^2 [-]
Mastic #0	0%	87.547	-1.7494	0.0861	-34.514	0.978
Mastic #1	25%	86.898	-1.5687	0.0927	-34.897	0.977
Mastic #2	50%	85.560	-1.5430	0.0933	-35.917	0.969
Mastic #3	75%	84.880	-1.0076	0.1205	-39.221	0.967
Mastic #4	100%	83.862	-0.9510	0.1197	-39.738	0.987

**Figure 8.** Master curves of asphalt mastics. (a) Complex shear modulus; (b) phase angle.

The complex shear modulus increased with the frequency; the phase angles performed a plateau zone at low-frequency zones and then decreased slightly. Asphalt mastics exhibited different rheological behaviors with varying the filler and frequency range. The ability of the asphalt mixture to resist deformation was reduced when FA replaced LF. Reducing δ at high temperatures was beneficial because it meant that FA improved the elastic behavior of mastics. However, the reduction in δ at low temperatures was unfavorable because FA also reduced the viscous behavior of mastics and increased the occurrence of low-temperature cracks.

3.3. Master Curve of Asphalt Mixtures

Figure 9a and 9b show G^* and δ for mixture #0 with varying temperatures, respectively.

**Figure 9.** Master curves of mixture #0. (a) Complex shear modulus; (b) phase angle.

The dynamic modulus of mixture #0 decreased with a frequency reduction or a temperature increase. Under a long-term load or high-temperature conditions, the internal

friction between the aggregate skeletons weakened and the material showed viscous characteristics [51]. As the load frequency decreased or temperature increased, the dynamic modulus of the asphalt mixture decreased, the asphalt viscosity increased, and the phase angle increased. At test temperatures of $-10\text{ }^{\circ}\text{C}$ and $4.4\text{ }^{\circ}\text{C}$, the trend in δ change for the mixtures aligned with the expected pattern. However, an anomaly was observed at $21.1\text{ }^{\circ}\text{C}$, where δ decreased with an increasing loading frequency, contrary to expectations. Similarly, at temperatures of $37.8\text{ }^{\circ}\text{C}$ and $54.4\text{ }^{\circ}\text{C}$, δ displayed trends that defied the anticipated behavior (Figure 9). This deviation can be attributed to the components of the asphalt mixtures (Figure 10).

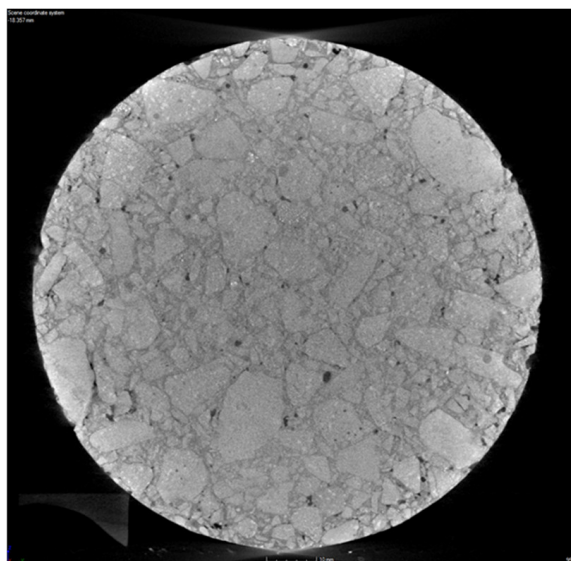


Figure 10. Scan photo of asphalt mixture.

Asphalt, as a temperature-sensitive viscoelastic material, will transform into a fluid at high temperatures and reduce its ability to resist deformation. Therefore, the composite viscoelastic properties of the asphalt mixture will undergo corresponding transformations. At low temperatures and high frequencies, the asphalt mortar affects the viscoelastic properties of the mixture. In contrast, at higher temperatures and lower frequencies, the asphalt mortar softens, and the impact of the mineral skeleton on the mixture's viscoelastic properties becomes significant. Given that mineral aggregates behave almost as ideal elastic materials with a nearly zero phase angle, the overall phase angle of the asphalt mixture exhibited a declining trend with a decreasing loading frequency.

Tables 6 and 7 list the fitting parameters of the master curves of G^* and δ of asphalt mixtures, respectively.

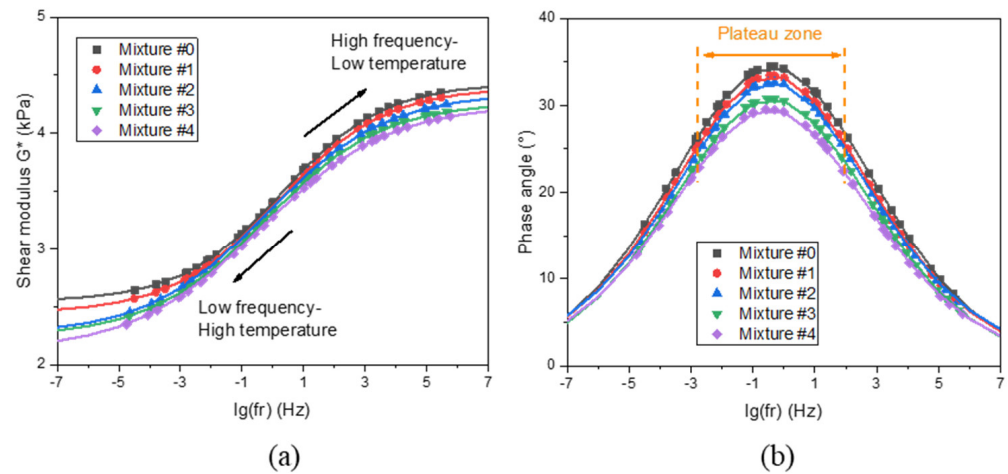
Table 6. Fitting parameters of master curves of G^* —asphalt mixtures.

Asphalt Mixture	FA Content [%]	$\lg\alpha$ [kPa]	β [kPa]	γ [-]	θ [-]	E_a [$\text{J}\cdot\text{mol}^{-1}$]	R^2 [-]
Mixture #0	0%	11.690	-0.0409	-0.2644	-4.2830	137,720	0.9986
Mixture #1	25%	11.018	0.0577	-0.2602	-4.2881	137,134	0.9986
Mixture #2	50%	10.934	-0.0071	-0.2430	-4.3313	136,914	0.9987
Mixture #3	75%	10.409	-0.0071	-0.2403	-4.8496	136,215	0.9986
Mixture #4	100%	1.8853	-0.1852	-0.4830	2.1199	137,720.0	0.9901

Correspondingly, the master curves of G^* and δ for asphalt mixtures are shown in Figures 11a and 11b, respectively.

Table 7. Fitting parameters of master curves of δ —asphalt mixtures.

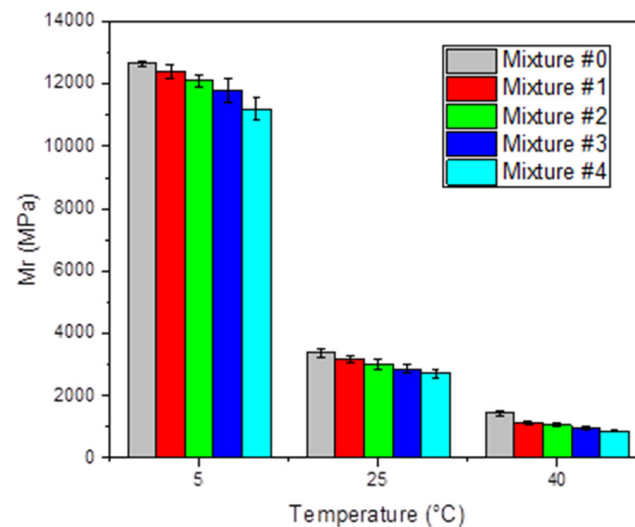
Asphalt Mixture	FA Content [%]	δ_P [°]	lgfP [Hz]	S_L [-]	S_R [-]	R^2 [-]
Mixture #0	0%	34.4776	0.4265	12.6456	−14.7866	0.907
Mixture #1	25%	33.4462	0.4208	11.1975	−12.2452	0.892
Mixture #2	50%	32.6620	0.4087	9.7683	−9.4306	0.892
Mixture #3	75%	30.7931	0.3952	9.4315	−8.8752	0.892
Mixture #4	100%	29.5642	0.3504	8.4593	−7.2625	0.894

**Figure 11.** Master curves of asphalt mixtures. (a) Complex shear modulus; (b) phase angle.

At each temperature and frequency, the G^* and δ of the SMA-13 with FA were smaller than those of mixture #0. Therefore, the effects of fly ash on the viscoelastic characteristics of asphalt materials presented a high consistency at the mastics scale and the mixture scale.

3.4. Resilient Modulus

The resilient modulus of asphalt mixtures revealed the effect of FA on the mechanical properties (Figure 12).

**Figure 12.** Resilient modulus of asphalt mixtures.

As the test temperature increased from 5 °C to 40 °C, the M_r of mixture #0 decreased from 12,651 MPa to 1442 MPa because the test temperature impacted the asphalt's viscoelastic properties. In addition, mixture #0 had a higher resilient modulus than mixtures with FA.

For example, the resilient modulus of the asphalt mixture at 25 °C reduced from 3374 MPa (Mixture #0) to 3196 MPa (Mixture #1), 3014 MPa (Mixture #2), 2854 MPa (Mixture #3), and 2730 MPa (Mixture #4). The LF exhibited strong interfacial bonding with asphalt, and FA resulted in the stripping of asphalt. Therefore, the increasing FA content would generate deterioration in the interfacial bonding strength and a reduction in the resilient modulus of the asphalt mixture.

3.5. Moisture Stability

Figure 13a shows the Marshall stability and flow value of asphalt mixtures; Figure 13b plots the Marshall modulus and immersion residual stability.

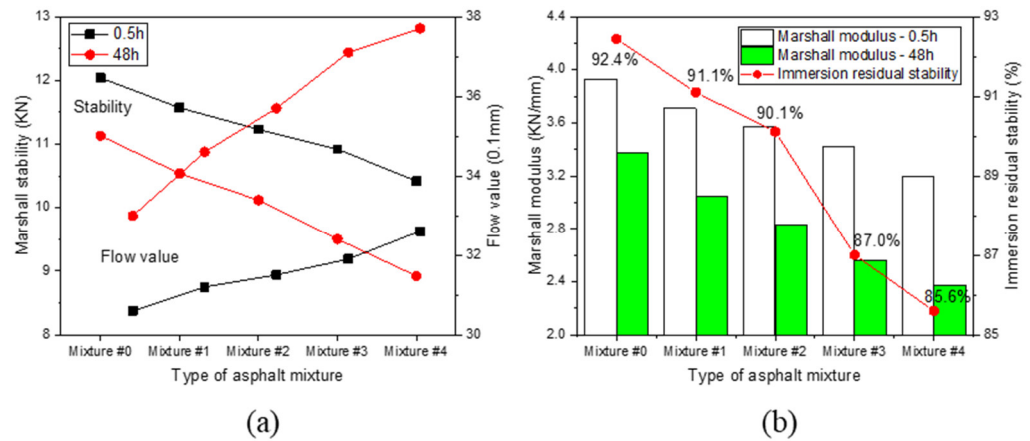


Figure 13. Marshall stability test: (a) Marshall modulus and flow values, (b) Immersion residual stability.

Whatever the bathing period, the addition of FA caused a decrease in Marshall stability and an increase in flow value (Figure 13a). Therefore, the Marshall modulus and immersion residual stability were reduced (Figure 13b), with an immersion residual stability decrease of 1.3% (Mixture #1), 2.3% (Mixture #2), 5.4% (Mixture #3), and 6.8% (Mixture #4), respectively.

3.6. Low-Temperature Performance

The bending test results are shown in Figure 14.

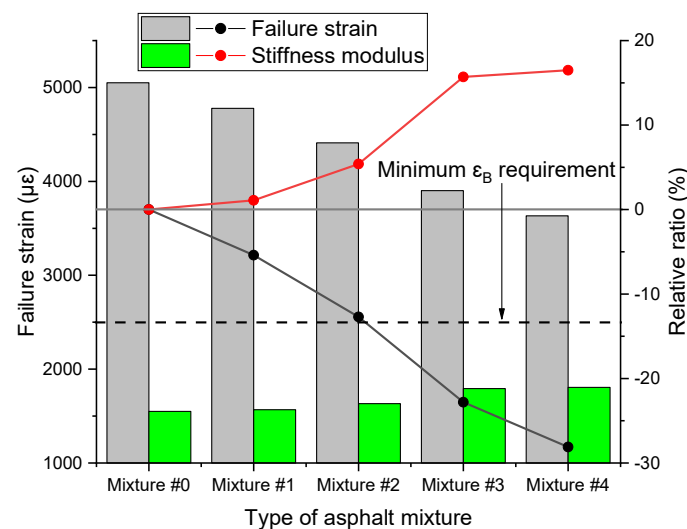


Figure 14. Bending test results at low temperature.

When FA completely replaced LF, the failure strain was reduced from 5051 $\mu\epsilon$ to 3633 $\mu\epsilon$, and the bending failure stiffness modulus was increased from 1550 MPa to 1805 MPa. All the mixtures complied [42] in terms of the minimum ϵ_B (i.e., 2500 $\mu\epsilon$).

4. Statistical Analyses

In this study, SPSS 2022 software was applied to perform a Pearson correlation test on viscoelastic parameters (i.e., α_T , γ , δ_p , lgf_p , S_L , and S_R in Figure 15a to Figure 15f, respectively) at asphalt mastic and mixture scales.

According to Figure 15, the viscoelastic parameters on the master curve of asphalt mastics were consistent with the results of the master curve of the asphalt mixture, presenting a strong correlation value (R^2 no less than 0.70). Moreover, the performance indices correlations confirmed the effect of FA on asphalt. Therefore, substituting mineral fillers significantly influences the viscoelastic characteristics and mechanical performances of asphalt materials at the mixture scale.

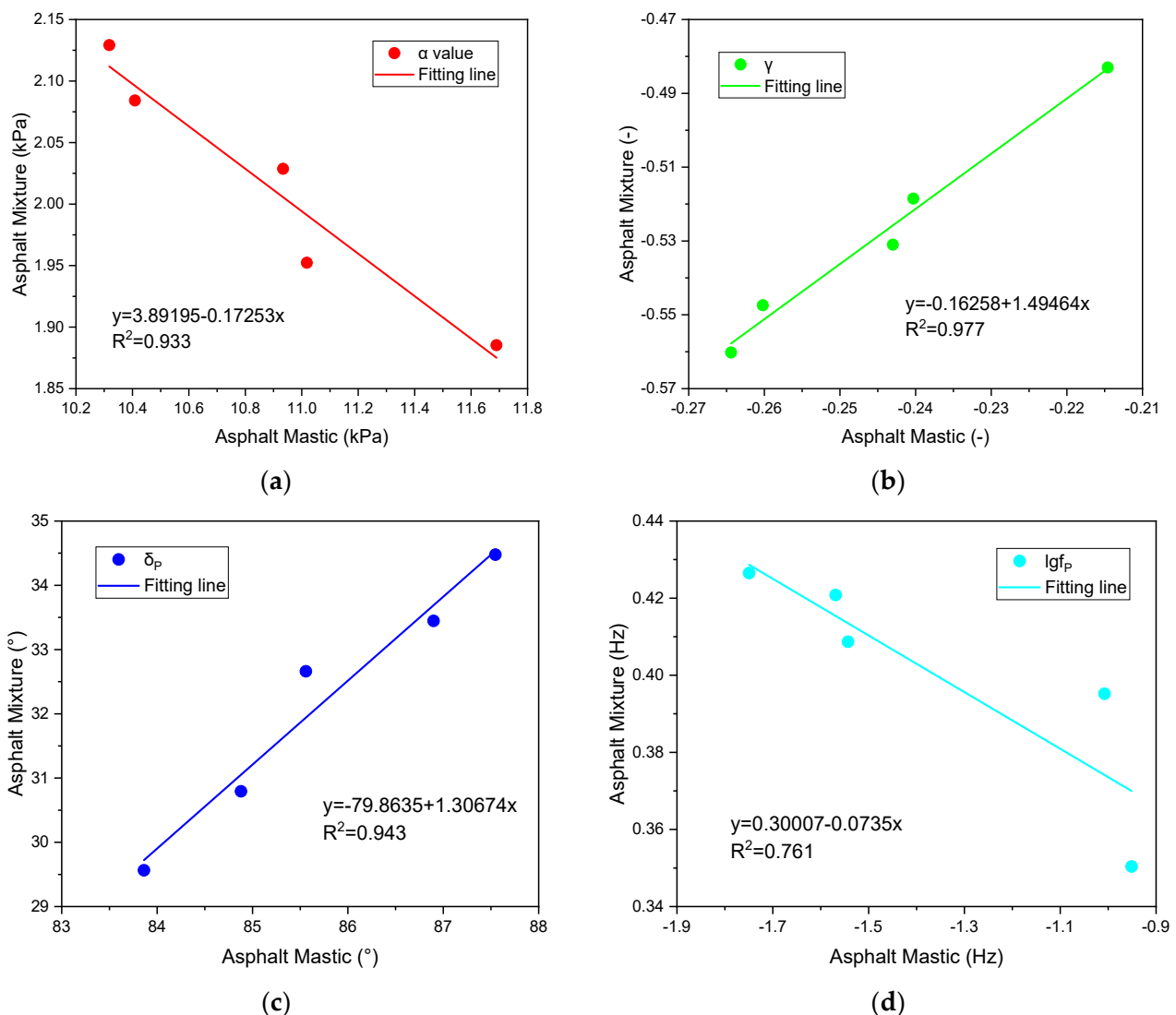


Figure 15. Cont.

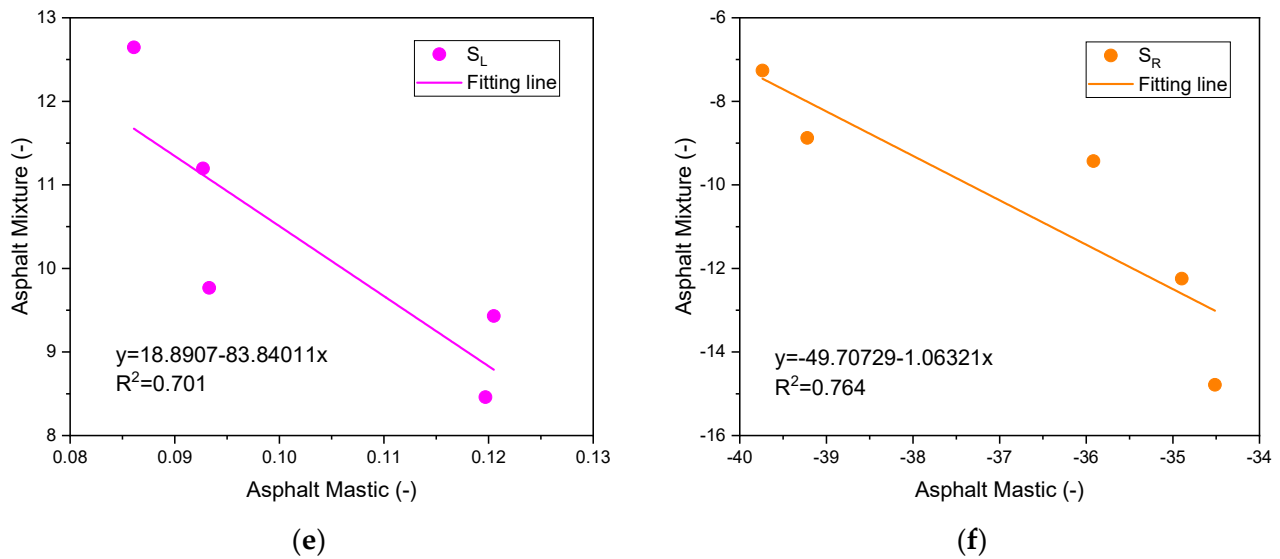


Figure 15. Correlation analysis of viscoelastic characteristics between asphalt mastics and asphalt mixtures: (a) α value, (b) γ value, (c) δ_P value, (d) $\lg f_P$ value, (e) S_L value, and (f) S_R value.

5. Conclusions

This study evaluated the feasibility of reusing fly ash from MSWIRs in asphalt pavements by investigating its viscoelastic characteristics and mechanical performances at different scales of mastic and mixture. Based on the findings, this research draws the following main conclusions:

1. Fly ash from MSWIRs and bitumen are physically blended without obvious chemical reactions during the modification process, indicating that fly ash exhibits compatibility with bitumen as a mineral powder;
2. The replacement of mineral powder by fly ash reduces the high- and low-temperature properties of the asphalt mixture. The activation energy of asphalt mixture required for deformation reduced from $208,069 \text{ J}\cdot\text{mol}^{-1}$ (Mixture #0) to $137,720 \text{ J}\cdot\text{mol}^{-1}$ (Mixture #4);
3. Fly ash improves the elastic component of asphalt mortar but reduces its ability to resist deformation and damage. The phase angle plateau value of asphalt mastics reduced from 87.547° (Mastic #0) to 83.862° (Mastic #4);
4. The immersion residual stability decreased by 7.40%. The incorporation of fly ash will reduce the moisture stability of the asphalt mixture;
5. Although the flexural tensile strength increased by 5.03%, the failure strain decreased by 41.15% and the stiffness modulus increased by 78.67%. The moisture stability and low-temperature performance of the mixture with FA can still meet the specification requirements of the asphalt layer;
6. There were strong correlations (R^2 over 0.70) between the viscoelastic parameters of asphalt mastics and mixtures. Substituting mineral fillers at the mastic scale significantly influences the viscoelastic characteristics and mechanical performances of asphalt materials at the mixture scale.

It is advisable for subsequent studies to engage in comprehensive long-term performance evaluations of the on-site test sections. Additionally, assessing the environmental impacts through detailed Life Cycle Assessment (LCA) methodologies will be crucial in understanding the broader ecological consequences.

Author Contributions: Conceptualization, L.X. and Y.D.; methodology, L.X. and S.B.; software, L.X. and Y.D.; validation, L.M. and G.L.; formal analysis, S.B. and L.M.; investigation, L.X., L.M. and S.B.; resources, Y.D.; data curation, L.X.; writing—original draft preparation, L.X. and G.L.; writing—review and editing, S.B. and L.M.; visualization, L.X.; supervision, Y.D.; project administra-

tion, Y.D.; funding acquisition, Y.D. All authors have read and agreed to the published version of the manuscript.

Funding: This research was funded by the National Natural Science Foundation of China (Grant number 51808562) and the Natural Science Foundation of Hunan Province, China (Grant number 2020JJ5723).

Data Availability Statement: The data presented in this study are available on request from the corresponding author.

Conflicts of Interest: The authors declare no conflicts of interest.

References

1. Abbà, A.; Collivignarelli, M.C.; Sorlini, S.; Bruggi, M. On the reliability of reusing bottom ash from municipal solid waste incineration as aggregate in concrete. *Compos. Part B Eng.* **2014**, *58*, 502–509. [[CrossRef](#)]
2. Du, Y.; Xu, L.; Deng, H.; Deng, D.; Ma, C.; Liu, W. Characterization of thermal, high-temperature rheological and fatigue properties of asphalt mastic containing fly ash cenosphere. *Constr. Build. Mater.* **2020**, *233*, 117345. [[CrossRef](#)]
3. Du, Y.; Ling, X.; Haibin, D.; Deyi, D.; Hao, W.; Weidong, L. Evaluation of thermal behavior and high-temperature performances of asphalt mixture containing fly ash cenosphere. *Constr. Build. Mater.* **2020**, *245*, 118429. [[CrossRef](#)]
4. Egemen, M.; Ali, F.; Aydin, E. An Approach to Mixture Design and Cost Analysis for Cement Pastes Composed of Class C Fly Ashes for Better Sustainable Construction. *Buildings* **2024**, *14*, 373. [[CrossRef](#)]
5. Win, T.T.; Wattanapornprom, R.; Prasittisopin, L.; Pansuk, W.; Pheinsusom, P. Investigation of Fineness and Calcium-Oxide Content in Fly Ash from ASEAN Region on Properties and Durability of Cement–Fly Ash System. *Eng. J.* **2022**, *26*, 77–90. [[CrossRef](#)]
6. Sereewatthanawut, I.; Panwisawas, C.; Ngamkhanong, C.; Prasittisopin, L. Effects of extended mixing processes on fresh, hardened and durable properties of cement systems incorporating fly ash. *Sci. Rep.* **2023**, *13*, 6091. [[CrossRef](#)]
7. Seraj, S.; Nikravan, M.; Ramezani-pour, A.A.; Zendehtdel, P. Evaluation of The Application of Municipal Solid Waste Incinerator (Mswi) Ash in Civil Engineering Using A Sustainability Approach. *Detritus* **2020**, *9*, 113–124. [[CrossRef](#)]
8. Vaitkus, A.; Škuldeckė, J.; Šernas, O. A Test Road with Unbound Base and Sub-Base Course from MSWI Bottom Ash Mixtures. *Buildings* **2023**, *13*, 1311. [[CrossRef](#)]
9. Allegrini, E.; Vadenbo, C.; Boldrin, A.; Astrup, T.F. Life cycle assessment of resource recovery from municipal solid waste incineration bottom ash. *J. Environ. Manag.* **2015**, *151*, 132–143. [[CrossRef](#)] [[PubMed](#)]
10. Dou, X.; Ren, F.; Nguyen, M.Q.; Ahamed, A.; Yin, K.; Chan, W.P.; Chang, V.W.-C. Review of MSWI bottom ash utilization from perspectives of collective characterization, treatment and existing application. *Renew. Sustain. Energy Rev.* **2017**, *79*, 24–38. [[CrossRef](#)]
11. Stabile, P.; Bello, M.; Petrelli, M.; Paris, E.; Carroll, M.R. Vitrification treatment of municipal solid waste bottom ash. *Waste Manag.* **2019**, *95*, 250–258. [[CrossRef](#)] [[PubMed](#)]
12. Cho, B.H.; Nam, B.H.; An, J.; Youn, H. Municipal Solid Waste Incineration (MSWI) Ashes as Construction Materials—A Review. *Materials* **2020**, *13*, 3143. [[CrossRef](#)] [[PubMed](#)]
13. Farina, A.; Kutay, M.E.; Anctil, A. Environmental assessment of asphalt mixtures modified with polymer coated rubber from scrap tires. *J. Clean. Prod.* **2023**, *418*, 138090. [[CrossRef](#)]
14. Paek, N.; Ri, S.; Jong, H.; Guo, Z. Study on production of cation asphalt emulsifier for micro-surfacing by using sulfomethylated lignin. *Int. J. Transp. Sci. Technol.* **2023**, *12*, 136–147. [[CrossRef](#)]
15. Balreddy, M.S.; Nethra, P.; Naganna, S.R. Performance Evaluation of Open-Graded Bituminous Concrete Modified with Natural Fibers. *Sustainability* **2023**, *15*, 11952. [[CrossRef](#)]
16. Hoy, M.; Horpibulsuk, S.; Arulrajah, A. Strength development of Recycled Asphalt Pavement–Fly ash geopolymer as a road construction material. *Constr. Build. Mater.* **2016**, *117*, 209–219. [[CrossRef](#)]
17. Hoy, M.; Horpibulsuk, S.; Rachan, R.; Chinkulkijniwat, A.; Arulrajah, A. Recycled asphalt pavement-fly ash geopolymers as a sustainable pavement base material: Strength and toxic leaching investigations. *Sci. Total Environ.* **2016**, *573*, 19–26. [[CrossRef](#)]
18. Kiihnl, L.; Braham, A. Exploring the influence of pavement preservation, maintenance, and rehabilitation on Arkansas’ highway network: An education case study. *Int. J. Pavement Eng.* **2021**, *22*, 570–581. [[CrossRef](#)]
19. Kumar, R.; Saboo, N.; Kumar, P.; Chandra, S. Effect of warm mix additives on creep and recovery response of conventional and polymer modified asphalt binders. *Constr. Build. Mater.* **2017**, *138*, 352–362. [[CrossRef](#)]
20. Liu, H.; Luo, R.; Xi, L.; Hu, L. Development of Two-Step Secant Method to Interpret the Flow Number Test Data of Asphalt Mixtures. *J. Mater. Civ. Eng.* **2020**, *32*, 111. [[CrossRef](#)]
21. Wang, C.; Zhang, H.; Castorena, C.; Zhang, J.; Kim, Y.R. Identifying fatigue failure in asphalt binder time sweep tests. *Constr. Build. Mater.* **2016**, *121*, 535–546. [[CrossRef](#)]
22. Wang, Z.; Zhou, H.; Mandapaka, V.; Nguyen, L. Pavement maintenance and rehabilitation practices in California: A study of 35-year as-built data in PaveM. *Int. J. Transp. Sci. Technol.* **2021**, *10*, 380–392. [[CrossRef](#)]

23. Mohammed, B.S.; Adamu, M.; Liew, M.S. Evaluating the effect of crumb rubber and nano silica on the properties of high volume fly ash roller compacted concrete pavement using non-destructive techniques. *Case Stud. Constr. Mater.* **2018**, *8*, 380–391. [[CrossRef](#)]
24. AASHTO. *Multiple Stress Creep Recovery (MSCR) Test of Asphalt Binder Using a Dynamic Shear Rheometer (DSR)*; AASHTO: Washington, DC, USA, 2012.
25. Wang, H.; Zhan, S.; Liu, G.; Xiang, J. The effects of asphalt migration on the flow number of asphalt mixture. *Constr. Build. Mater.* **2019**, *226*, 442–448. [[CrossRef](#)]
26. NCHRP. *Simple Performance Test for Superpave Mix Design*; Transportation Research Board: Washington, DC, USA, 2002; Volume 465.
27. Xu, L.; Du, Y.; Loprencipe, G.; Moretti, L. Rheological and Fatigue Characteristics of Asphalt Mastics and Mixtures Containing Municipal Solid Waste Incineration (MSWI) Residues. *Sustainability* **2023**, *15*, 8356. [[CrossRef](#)]
28. Wang, Y.; Li, W. Study on High Temperature Performance of Asphalt Mixture Based on Rutting Test. *AMM* **2015**, *744–746*, 1316–1319. [[CrossRef](#)]
29. Zhou, F.; Scullion, T.; Sun, L. Verification and Modeling of Three-Stage Permanent Deformation Behavior of Asphalt Mixes. *J. Transp. Eng.* **2004**, *130*, 486–494. [[CrossRef](#)]
30. Babagoli, R.; Ameli, A.; Asadi, S. Effects of copolymers on rheological and performance of binders and stone matrix asphalt mixtures. *Int. J. Pavement Eng.* **2022**, *1*, 2124250. [[CrossRef](#)]
31. Xu, L.; Li, X.; Zong, Q.; Xiao, F. Chemical, morphological and rheological investigations of SBR/SBS modified asphalt emulsions with waterborne acrylate and polyurethane. *Constr. Build. Mater.* **2021**, *272*, 121972. [[CrossRef](#)]
32. Liu, Z.; Zhou, Z.; Gu, X.; Sun, L.; Wang, C. Laboratory evaluation of the performance of reclaimed asphalt mixed with composite crumb rubber-modified asphalt: Reconciling relatively high content of RAP and virgin asphalt. *Int. J. Pavement Eng.* **2023**, *24*, 2217320. [[CrossRef](#)]
33. Aysen Lav, M.; Hilmi Lav, A. Effects of stabilization on resilient characteristics of fly ash as pavement material. *Constr. Build. Mater.* **2014**, *54*, 10–16. [[CrossRef](#)]
34. Stel'makh, S.A.; Shcherban', E.M.; Beskopylny, A.N.; Mailyan, L.R.; Meskhi, B.; Shilov, A.A.; Evtushenko, A.; Chernil'nik, A.; El'shaeva, D.; Karalar, M.; et al. Physical, Mechanical and Structural Characteristics of Sulfur Concrete with Bitumen Modified Sulfur and Fly Ash. *J. Compos. Sci.* **2023**, *7*, 356. [[CrossRef](#)]
35. Özkılıç, Y.O.; Çelik, A.İ.; Tunç, U.; Karalar, M.; Deifalla, A.; Alomayri, T.; Althoey, F. The use of crushed recycled glass for alkali activated fly ash based geopolymer concrete and prediction of its capacity. *J. Mater. Res. Technol.* **2023**, *24*, 8267–8281. [[CrossRef](#)]
36. Karalar, M. Experimental and Numerical Investigation on Flexural and Crack Failure of Reinforced Concrete Beams with Bottom Ash and Fly Ash. *Iran J. Sci. Technol. Trans. Civ. Eng.* **2020**, *44*, 331–354. [[CrossRef](#)]
37. Du, S. Effect of curing conditions on properties of cement asphalt emulsion mixture. *Constr. Build. Mater.* **2018**, *164*, 84–93. [[CrossRef](#)]
38. Grilli, A.; Graziani, A.; Bocci, M. Compactability and thermal sensitivity of cement-bitumen-treated materials. *Road Mater. Pavement Des.* **2012**, *13*, 599–617. [[CrossRef](#)]
39. Fang, X.; Garcia, A.; Winnefeld, F.; Partl, M.N.; Lura, P. Impact of rapid-hardening cements on mechanical properties of cement bitumen emulsion asphalt. *Mater. Struct.* **2016**, *49*, 487–498. [[CrossRef](#)]
40. Gómez-Meijide, B.; Pérez, I. A proposed methodology for the global study of the mechanical properties of cold asphalt mixtures. *Mater. Des.* **2014**, *57*, 520–527. [[CrossRef](#)]
41. *JTG E42-2005*; Test Methods of Aggregate for Highway Engineering. Chinese Standard: Beijing, China, 2005.
42. *JTG E20-2011*; Standard Test Methods of Bitumen and Bituminous Mixtures for Highway Engineering. Chinese Standard: Beijing, China, 2011.
43. *JTG F40-2004*; Technical Specifications for Construction of Highway Asphalt Pavements. Chinese Standard: Beijing, China, 2004.
44. Xu, L.; Alae, M.; Du, Y.; Loprencipe, G.; Peluso, P.; Moretti, L. Thermal Characteristics and Temperature Distribution of Asphalt Mixtures Containing Residues from Municipal Solid Waste Incineration. *Sustainability* **2023**, *15*, 15612. [[CrossRef](#)]
45. *AASHTO TP62-07*; Standard Method of Test for Determining Dynamic Modulus of Hot-Mix Asphalt Concrete Mixtures. AASHTO: Washington, DC, USA, 2007.
46. Hassan, M.M.; Khalid, H.A. Compressive Deformation Behaviour of Asphalt Mixtures Containing Incinerator Bottom Ash Aggregate. *Road Mater. Pavement Des.* **2010**, *11*, 633–652. [[CrossRef](#)]
47. *ASTM D7369-20*; Standard Test Method for Determining the Resilient Modulus of Asphalt Mixtures by Indirect Tension Test. ASTM: West Conshohocken, PA, USA, 2020.
48. Ziyani, L.; Gaudefroy, V.; Ferber, V.; Hammoum, F. A predictive and experimental method to assess bitumen emulsion wetting on mineral substrates. *Colloids Surf. A Physicochem. Eng. Asp.* **2016**, *489*, 322–335. [[CrossRef](#)]
49. Zhao, W.; Yang, Q. Life cycle assessment and multi-index performance evaluation of semi-flexible pavement after composite modification by using fly ash, rubber particles, warm mixing asphalt and recycled asphalt pavement. *Constr. Build. Mater.* **2023**, *364*, 129945. [[CrossRef](#)]

50. Bruno, S.; Del Serrone, G.; Di Mascio, P.; Loprencipe, G.; Ricci, E.; Moretti, L. Technical Proposal for Monitoring Thermal and Mechanical Stresses of a Runway Pavement. *Sensors* **2021**, *21*, 6797. [[CrossRef](#)] [[PubMed](#)]
51. Gambalunga, B.; Nicolini, J.L.; Inocente, J.M.; Pich, C.T.; Angioletto, E.; Pereira, F.R.; Montedo, O.R.K.; Arcaro, S. Valorization of waste foundry sand aggregates in hot-mix asphalt. *Process Saf. Environ. Prot.* **2023**, *173*, 277–288. [[CrossRef](#)]

Disclaimer/Publisher’s Note: The statements, opinions and data contained in all publications are solely those of the individual author(s) and contributor(s) and not of MDPI and/or the editor(s). MDPI and/or the editor(s) disclaim responsibility for any injury to people or property resulting from any ideas, methods, instructions or products referred to in the content.